We are IntechOpen, the world's leading publisher of Open Access books Built by scientists, for scientists

4,800
Open access books available

122,000
International authors and editors

135M
Downloads

Our authors are among the

154
Countries delivered to

TOP 1%
most cited scientists

12.2%
Contributors from top 500 universities

CLARIVATE ANALYTICS BOOK CITATION INDEX INDEXED

WEB OF SCIENCE™

Selection of our books indexed in the Book Citation Index in Web of Science™ Core Collection (BKCI)

Interested in publishing with us?
Contact book.department@intechopen.com

Numbers displayed above are based on latest data collected.
For more information visit www.intechopen.com

28

Synthesis and Characterisation of Silica/Polyamide-Imide Composite Film for Enamel Wire

Xiaokun Ma and Sun-Jae Kim*
Institute/Faculty of Nanotechnology and Adv. Materials Engin., Sejong University #98 Gunja-dong, Gwangjin-gu, Seoul, South Korea

1. Introduction

In the past decade, the demand for polyamide-imide (PAI) and other high-temperature resistant polymeric materials has grown steadily because of their outstanding mechanical properties and excellent thermal and oxidative stability (Zhong, 2002; Sun, 2006; Yanagishita, 2001; Babooram, 2008). PAI is well-known for its low thermal expansion coefficient and dielectric constant. In microelectronics, PAI has been widely used as an inter-dielectric material, and in the large-scale integrated circuit industry, as an electrical insulation for conventional appliances (Kawakami, 1996, 1998, 2003; Rupnowski, 2006; Wu, 2005). Compared with pure polyimide and polyamide, PAI exhibits better process ability and heat-resistant properties. The application of PAI as a wire-coating material with thermal-resistant properties has attracted increasing interest (Chen, 1997; Ranade, 2002; Ma, 2007). However, with the introduction of higher-surge voltage devices, an increasing number of insulation electric breakdown cases have been reported. Insulation electric breakdown must be prevented because it may lead to electrical component failure or may endanger the people handling the component. Thus, the development of an organic/inorganic composite insulating material is essential in designing insulation for continuous use (Alexandre, 2000; Hossein, 2007; David, 1995; Yang, 2006). Polymer composites have received much attention, as various properties of the original matrix polymer can be considerably improved by adding a limited percentage of inorganic filler (Jiao, 1989; Rangsunvigit, 2008; Xu, 2007; Hwang, 2008; Kim, 2007; Rankin, 1998).

Silica has been commonly used as an inorganic component because it is effective in enhancing the mechanical and thermal properties of polymers. Various studies on the preparation of polymer/silica composite films have been conducted (Butterworth, 1995; Mosher, 2006; Kim, 2006; Ahn, 2006; Stathatos, 2004).

The properties of hybrid composites are affected by many factors, such as particle size, size distribution, and filler content. In addition, the inorganic particle shape, surface structure,

* Corresponding Author

and mechanical properties of a filler (stiffness and strength, among others) play important roles in inorganic/organic composite material synthesis. In particular, the bond strength between the inorganic particles and the polymer matrix, influenced by the dispersion aid type or coupling agent used, should be improved (Kusakabe, 1996; Fuchigami, 2008; Castellano, 2005; Alexandre, 2000; Wu, 2006; Zheng, 2007; Ohki, 2005).

Silica nanoparticles, as important inorganic materials, have emerged as an area of intense interest because of their special physical and chemical properties, such as their small size, strong surface energy, high scattered performance, and thermal resistance (Ouabbas, 2009; Lee, 2006; Bhagat, 2008; Oh, 2009; Xue, 2009). However, the applications of silica nanoparticles are largely limited because of their highly energetic hydrophilic surface, which causes the silica nanoparticles to easily agglomerate. Surface modification methods using different surfactant agents may resolve this limitation. Thus, the strong interface adhesion between the organic matrix and the silica nanoparticles is the key to the application of silica nanoparticles as fillers.

Jadav et al. successfully synthesised a silica/polyamide nanocomposite film via interfacial polymerisation using two types of silica nanoparticles of 16 and 3 nm in size (Jadav, 2009). The nanocomposite films exhibited superior thermal stability to the pure polyamide membranes. In the current work, silica nanoparticle loading significantly modified the polyamide network structure, pore structure, and transport properties. The excellent membrane performance in terms of separation efficiency and productivity flux was also discussed. Zhang et al. prepared a novel isometric polyimide/silica hybrid material via sol-gel technique (Zhang, 2007). Initially, 3-[(4-phenylethynyl) phthalimide] propyl triethoxysilane was synthesised to modify the nanosilica precursor. Then, the isomeric polyimide/silica hybrid material was produced using isomeric polyimide resin solution and the modified nanosilica precursor after heat treatment. The isomeric polyimide/silica composite has much better thermal properties and nano-indenter properties than those of the isomeric polyimide.

In the current work, the commercial silica nanoparticles and self-synthesised spherical silica particles were successfully dispersed in the PAI polymer matrix after the surface modification process. The cationic surfactant cetyltrimethyl ammonium bromide (CTAB) was chosen to modify the silica nanoparticles. The amount of CTAB added in modifying the silica nanoparticles was increased from 0 to 3 wt%. After the surface modification process, the CTAB-modified silica nanoparticles showed better compatibility with the PAI polymer matrix. The results indicate that CTAB plays an important role in the preparation of silica/PAI composite film. The thermal stability improved and the decomposition temperature increased with increasing amounts of silica particles. The thermal expansion coefficient of the composite film was lower than that of the PAI polymer matrix, which is helpful in extending the life of the enameled wire.

2. Synthesis and characterisation of the spherical silica/PAI composite film

Spherical silica/PAI composite films have been successfully prepared via simple ultrasonic blending. In the current study, the spherical silica particles were prepared according to the Stőber procedure, and the size was controlled to approximately 300 nm at room temperature. After the surface modification process, the commercial silica nanoparticles and

the self-synthesised spherical silica particles were dispersed in separate PAI polymer matrices. The correlation of the silica particle size with the amount of silica dispersed in the PAI under optimal experimental conditions was discussed.

2.1 Preparation of the silica/PAI composite film

2.1.1 Synthesis of the spherical silica submicron particles

The spherical silica particles were prepared according to the Stőber procedure, which allows the preparation of monodispersed silica particles with particle sizes in the nanometer to submicron range. A 500 ml three-necked flask equipped with a mechanical stirrer was filled with 45 ml ethanol, 2 ml NH_3 H_2O, and 1 ml deionised H_2O. The spherical silica synthesis was initiated by the rapid addition of 2 ml tetra-ethoxy-silane (TEOS) to a stirred solution. After the mixture was vigorously stirred for 2 h, spherical silica submicron particles of approximately 300 nm in size, were obtained at room temperature. Then, the silica particles were centrifuged at 10000 rpm for 30 min. The resultant silica particles were washed with ethanol and distilled H_2O, and then modified with CTAB.

2.1.2 Surface modification of the silica particles

CTAB can be directly added into the submicron silica solutions, and the CTAB amount can be increased from 0 to 3wt % at the optimal temperature of 60 °C. After the surface modification process, the modified silica particles were collected via centrifugation and then dried at 60 °C.

In the experiment, 100 ml deionised H_2O and 1 g commercial silica nanoparticles were added to a flask and the solution was adjusted to pH 8 by the addition of 0.1 M NaOH. The silica nanoparticles were modified at 65 °C with the addition of CTAB under constant stirring. The dispersal state of the silica nanoparticles in the PAI matrix was improved by increasing the amount of CTAB from 0 to 3.0 wt%. After the surface modification process, the modified nanosilica particles were collected via suction filtration and then dried at 90 °C for 6 h.

2.1.3 Preparation of the silica/PAI composite film

The nanosilica/PAI composite films were prepared via simple ultrasonic blending. Two grams of PAI powder were dissolved in 3 ml N,N-dimethyl form amide (DMF). The silica nanoparticles were added into the solution, and the amount of silica was increased from 2 to 10 wt%. The mixture was put under ultrasonic dispersion for approximately 3 h at room temperature. The mixture solution was then cast on a square glass plate (5 cm × 5 cm) using a bar coater. Bar coaters are primarily used in applying a variety of coatings or emulsions to a multitude of substrates. The bar coater used in the current experiment had a 0.2 mm diameter and was made of stainless steel wire, which resulted in more uniform silica/PAI composite films. The films were initially heated to remove the solvent in the vacuum oven. The temperature was controlled as follows: at 60 °C for 4 h, at 80 °C for 2 h, increased to 120 °C for 1 h, and finally, kept at 160 °C for 1 h. The experimental details of the silica/PAI composite film preparation are shown in Scheme 1.

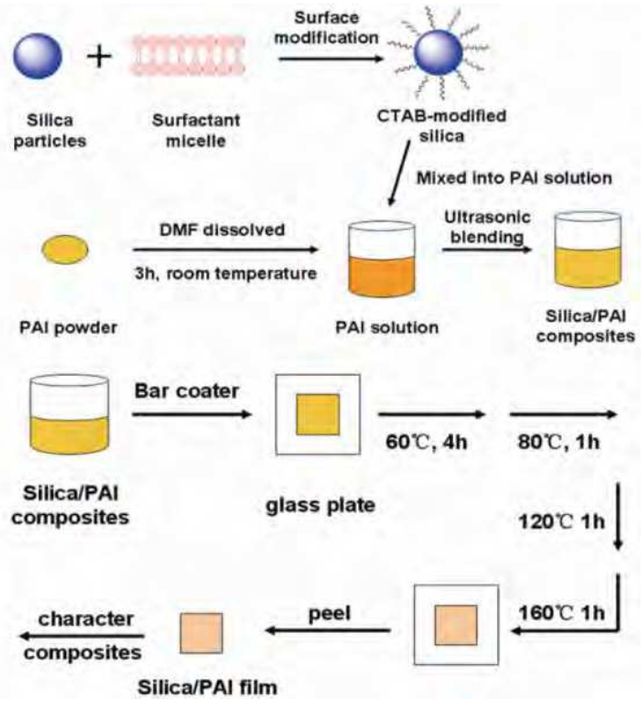

Scheme 1. Preparation of the silica/PAI nanocomposite films.

The spherical silica/PAI composite films were obtained under the same method. Spherical submicron silica particles do not easily agglomerate, so the amount of submicron silica added to PAI in the system was increased to 25%. The reactants of the submicron silica/PAI composites are listed in Table 1.

Reactant Sample	Silica Particles (g)	PAI (g)	DMF (ml)	Theoretical Weight Percent (wt%)
Composite 1	0.04	2.0	3	1.96
Composite 2	0.08	2.0	3	3.85
Composite 3	0.12	2.0	3	5.66
Composite 4	0.16	2.0	3.5	7.41
Composite 5	0.20	2.0	3.5	9.10
Composite 6	0.30	2.0	3.5	13.0
Composite 7	0.40	2.0	4	16.7
Composite 8	0.50	2.0	4	20.0

Table 1. Reactants of the different submicron silica/PAI composite samples.

2.2 Characterisation of the silica/PAI composite film

The fracture surfaces of the composite films were studied using a scanning electron microscope (SEM Hitachi S-4700, Hitachi Co.). Prior to SEM imaging, the samples were sputtered with thin layers of Pt-Pd. The silica/PAI nanocomposite films were characterised

by an FT-IR (OMNIC NICOLET 380) spectrometer. The spectra were measured in the range 4000–650 cm^{-1}. A Scinco STA S-1500 simultaneous thermal analyser was then used to analyse the thermal stability of the nanosilica/PAI composite films. The samples were heated from 30 to 800 °C at 10 °C/min under air atmosphere. The coefficients of thermal expansion (CTE) of the silica/PAI composites films were evaluated using a Q 400 EM (U.S.A) thermomechanical analyser (5 °C/min from 25 to 300 °C, 50 mN). All the samples were 3 mm × 16 mm, cut from the original films using a razor blade.

2.2.1 CTAB effect on the synthesis of silica/PAI composite film

The FT-IR spectra of the silica/PAI composite films are shown in Fig. 1. The effect of the surfactant on the composite films was evaluated by increasing the CTAB dosage from 0 to 3 wt%. The amount of silica nanoparticles added to the PAI was 6 wt%. The character vibrations of the Si-O were observed at 1086, 945, and 796 cm^{-1}, as shown in Fig. 1 (e). After the surface modification process, the typical stretching vibrations of the C-H were found at 2855 and 2928 cm^{-1}, which resulted from the $-CH_2$ and $-CH_3$ in the CTAB. Figure 1 shows the typical characteristic bands of the PAI polymer matrix that were found, such as the N-H stretching band at 3317 cm^{-1}, the amide C=O region at around 1710 cm^{-1}, and the bands at 1771 and 1710 cm^{-1} associated with the imide carbonyl band. The bands are similar to one another because the same amount of silica was added into the composites. The characteristic stretching vibration of Si-O at 1086 cm^{-1} became wider when the silica nanoparticles were modified by CTAB. This peak broadening may be explained by the organic side-chain of CTAB grafted on the surface of the silica nanoparticles, which improved the interaction between the silica nanoparticles and the PAI polymer matrix.

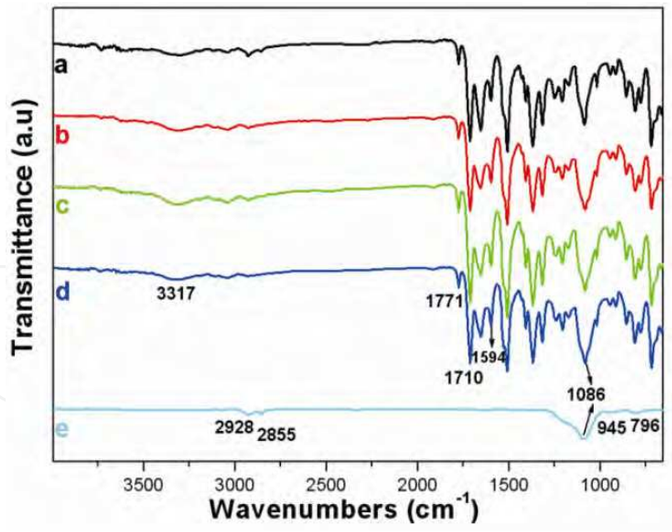

Fig. 1. FT-IR spectra of (a) unmodified-silica/PAI nanocomposites, (b) 1% CTAB-silica/PAI nanocomposites, (c) 2% CTAB-silica/PAI nanocomposites, (d) 3% CTAB-silica/PAI nanocomposites, and (e) CTAB-modified silica nanoparticles.

The fracture surface micrographs of the silica/PAI nanocomposite films are shown in Fig. 2. In Fig. 2 (a), some silica agglomerations are found in the micrograph when the unmodified-silica nanoparticles were added into the PAI matrix. The silica nanoparticles easily

agglomerate because of their large surface-to-volume ratios and high surface tension. However, the CTAB-modified silica nanoparticles dispersed well in the PAI matrix with the increase in CTAB. The dispersal state of the silica nanoparticles improved when the silica nanoparticles were modified with 1 wt% CTAB, as shown in Fig. 2 (b). In Fig. 2 (c), the silica nanoparticles are almost monodispersed, and little agglomeration is observed when 2 wt% CTAB-modified silica nanoparticles were added into the PAI polymer. After the silica were modified with 3 wt% CTAB, the silica nanoparticles became monodispersed without any agglomerations, although the amount of silica nanoparticles added to the PAI was increased to 6 wt%, as shown in Fig. 2 (d). CTAB improves the dispersal state of the silica nanoparticles in a PAI polymer matrix, with an optimal dosage of 3 wt%.

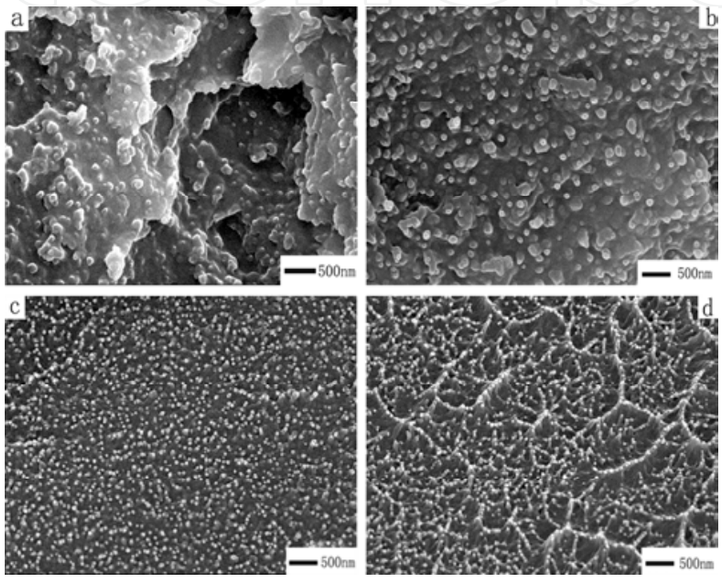

Fig. 2. Fracture surface micrographs of (a) unmodified-silica/PAI nanocomposites, (b) 1% CTAB-silica/PAI nanocomposites, (c) 2% CTAB-silica/PAI nanocomposites, and (d) 3% CTAB-silica/PAI nanocomposites.

Fig. 3 shows the thermogravimetric analysis (TGA) plots of the different CTAB modified-silica/PAI nanocomposites films when 6 wt% nanosilica was added into the PAI matrix. Some differences are found in the weight loss curves shown in Fig. 3. When the temperature was increased to 475 °C, the silica/PAI composites began to decompose. Compared with the unmodified-silica/PAI composites, the decomposition temperature increased after the silica nanoparticles were modified by CTAB. The results indicate that the CTAB-modified silica particles improve the thermal stability of the PAI polymer matrix. In addition, the decomposition temperature of composite films increased with increasing CTAB dosage. When the amount of CTAB added to the silica was increased from 0 to 3 wt%, the decomposition temperature of the composite films increased from 646 to 658, 671, and 682 °C, respectively. A thermal decomposition process occurs when the temperature approaches 595 °C, as shown in Figs. 3 (b)-(d). Therefore, the interaction between the silica nanoparticles and PAI polymer matrix is enhanced after the silica are modified by CTAB.

CTAB improves not only the dispersal state of silica in the PAI matrix, but also the thermal stability of the composite film because of the better interaction between the nanosilica and

PAI matrix. The amount of silica in the composites was calculated based on the plots, and the result was about 5.6 wt%, which is in accordance with the theoretical data.

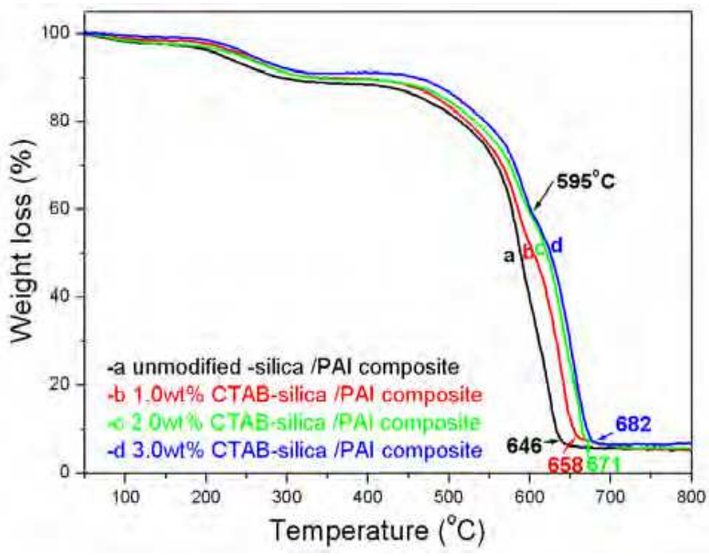

Fig. 3. TGA plots of (a) unmodified-silica/PAI nanocomposites, (b) 1% CTAB-silica/PAI nanocomposites, (c) 2% CTAB-silica/PAI nanocomposites, and (d) 3% CTAB-silica/PAI nanocomposites.

Thus, CTAB, with an optimal dosage of 3 wt%, was chosen to modify the nanosilica. The fracture surface micrographs of the composites show that the silica nanoparticles were well-dispersed in the PAI matrix after the surface modification process. In the TGA plots of the silica/PAI nanocomposites, the thermal stability and the decomposition temperature increased with increasing CTAB. Therefore, CTAB is important in the preparation of the silica/PAI nanocomposite film.

2.2.2 The effect of silica nanoparticle amount on the properties of silica/PAI composite film

The FT-IR spectra of the pure PAI and some silica/PAI nanocomposite films are shown in Fig. 4 The amount of silica nanoparticles added to PAI was changed from 2 to 10 wt%, and the dosage of CTAB added to the silica was 3 wt%. In the spectra shown in Fig. 4, the bands at 1771 and 1710 cm^{-1} are associated with the imide carbonyl band. Both bands are insensitive to the presence of the silica nanoparticles. The bands in the region from 945 to 650 cm^{-1} increased with the increase in silica content, caused by the presence of a broad band associated with the vibration of the Si-O bond. The N-H stretching band at 3317 cm^{-1} was slightly intensified with the increase in silica content, indicating the hydrogen-bonded N-H groups in the PAI polymer and the Si-O-Si or Si-O-H groups of the silica nanoparticles. The characteristic band at 1594 cm^{-1} comes from the benzene-ring stretch and a contribution from the O-H bond in monomeric H_2O, which also has a band at 1663 cm^{-1}. All the characteristic peaks in the composites indicate that the interaction between the silica nanoparticles and PAI polymer matrix is sensitive to the amount of silica in the composites.

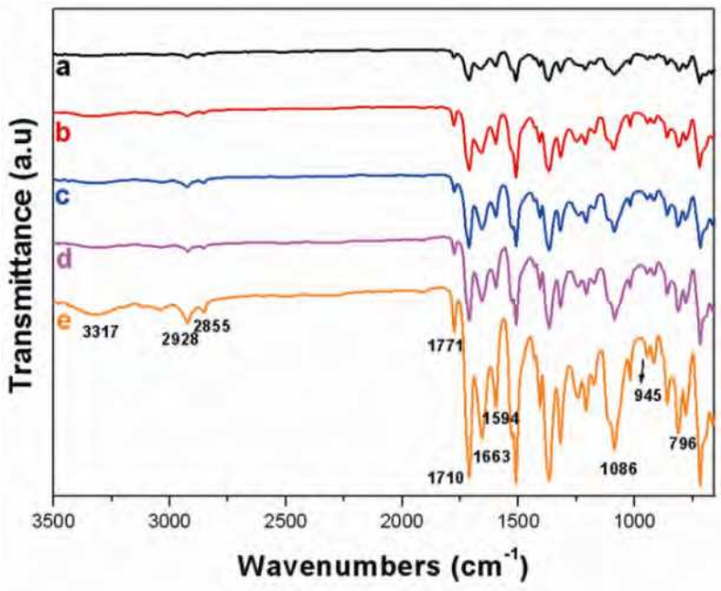

Fig. 4. FT-IR spectra of the silica/PAI composites with the amount of silica nanoparticles added to PAI at (a) 2 wt%, (b) 4 wt%, (c) 6 wt%, (d) 8 wt%, and (e) 10 wt%.

The fractured surface micrographs of the pure PAI and several composite films are shown in Fig. 5. The fracture surfaces of the pure PAI film are uniform, and the continuous polymer phase is shown in Fig. 5 (a). Figs. 5 (b)–(f) show the fracture surfaces of the different silica/PAI composites. The amount of silica added to the PAI was increased from 2 to 10 wt%. The larger the amount of silica nanoparticles added to the PAI, the greater their amount found in the fracture surface micrographs. In Fig. 5 (f), when 10 wt% silica nanoparticles was added into the PAI, the silica nanoparticles remained monodispersed without any agglomerations. The results indicate that the CTAB-modified silica nanoparticles have better dispersal state in the PAI polymer matrix. In addition, the CTAB-modified silica nanoparticles increased the silica nanoparticle content in the composites. Thus, the surface modification process is an effective method of preparing silica/PAI nanocomposites.

The thermal stability of the silica/PAI composite films was evaluated via TGA. The TGA plots of the PAI and the composites with the different amounts of silica nanoparticles are shown in Fig. 6. The amount of silica nanoparticles added to the PAI polymer matrix was increased from 0 to 10 wt%. The plots are shown in Figs. 6 (a)–(f). A weight loss is observed above 170 °C on all the TGA plots, which corresponds to water and solvent losses. When the temperature was increased to 450 °C, the PAI matrix began to decompose. The decomposition temperature increased when the silica nanoparticles were added into the PAI polymer matrix. At the same temperature, all the curves of the composites indicated that the composite weight loss was less than that of the pure PAI matrix. The silica/PAI composites have higher decomposition temperature when the PAI polymer matrix loses the same weight. The thermal stability of PAI was enhanced with the increase in the silica content. The amount of silica nanoparticles in the composites were calculated accurately in the TGA plots. The silica content in the composites based on Figs. 6 (b)–(f) are 1.9, 3.6, 5.8, 7.3, and 10.2 wt%, respectively.

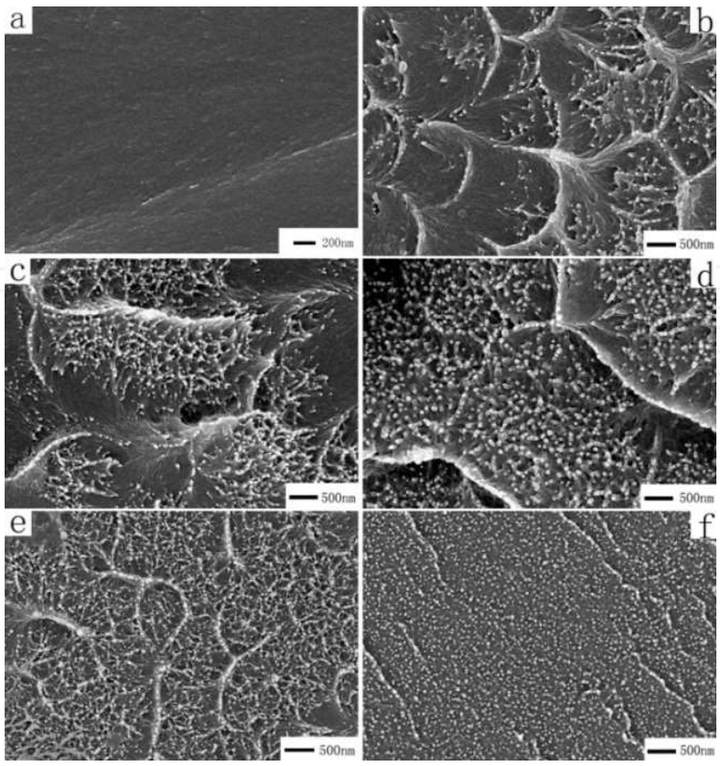

Fig. 5. Fracture surface micrographs of (a) pure PAI and silica/PAI nanocomposite, with the amount of silica added to PAI at (b) 2 wt%, (c) 4 wt%, (d) 6 wt%, (e) 8 wt%, and (f) 10 wt%.

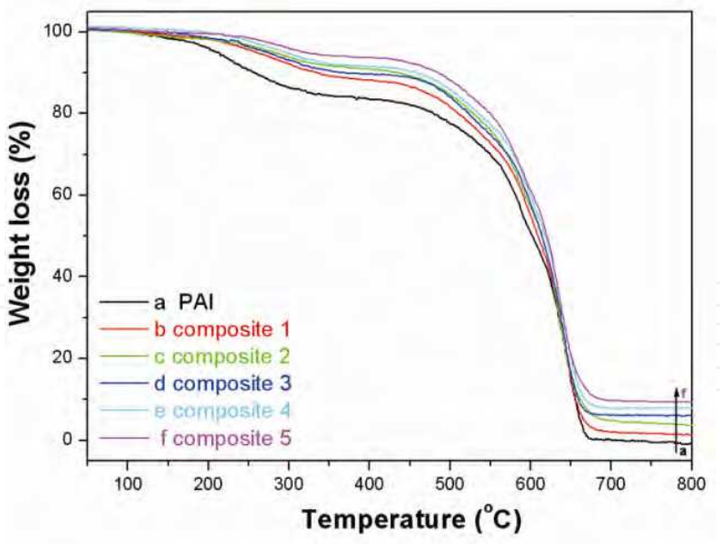

Fig. 6. TGA plots of the (a) PAI matrix, and the silica/PAI nanocomposite films with the amount of silica added to PAI at (b) 2 wt%, (c) 4 wt%, (d) 6 wt%, (e) 8 wt%, and (f) 10 wt%.

CTE is an important parameter in evaluating the properties of enamel wire. A low CTE can reduce thermal stress build-up and prevent device failure through peeling and cracking at the interface between the polymer film and the copper. The CTE curves of the pure PAI film

and some composite films are shown in Fig. 7. The CTE value of the PAI films was 3.87 × 10^{-5} m/m/°C, whereas that of the silica/PAI composite film decreased to 3.69 × 10^{-5} and 3.51 × 10^{-5}m/m/°C when the amount of silica added to PAI was 4 and 6 wt%, respectively. The CTE values continuously decreased with increasing amount of the silica particles. In particular, the CTE value decreased to 3.35 × 10^{-5} m/m/°C when the amount of silica added to PAI was 10 wt%, as shown in Fig. 7 (d). Compared with the PAI polymer film, the silica/PAI composite films had lower CTE, which may be attributed to the rigidity and stiffness of the silica nanoparticles and the interaction between the silica and PAI polymer matrix. The rigidity and stiffness of the silica nanoparticles limit the polymer chain movement, resulting in the decrease of the PAI matrix thermal expansion.

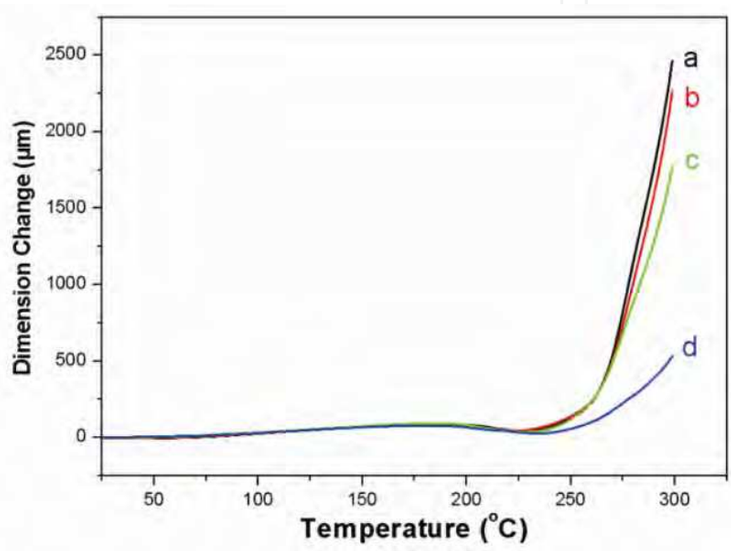

Fig. 7. CTE curves of the (a) pure PAI film and the composite films with silica content at (b) 4 wt%, (c) 6 wt%, and (d) 10 wt%.

The thermal stability of the silica/PAI nanocomposites improved and the decomposition temperature increased when the amount of silica nanoparticles was increased. The lower CTE of the composite films can reduce the peeling and cracking at the interface between the polymer film and the copper. In the current system, the high thermal stability and low CTE show that the silica/PAI nanocomposite films can be widely used in the enamel wire industry.

2.2.3 Effect of silica diameter on the properties of the silica/PAI composite film

In the past years, innovative inorganic/organic composite technology has been used to develop wires with better inverter-surge-resistance and mechanical properties than those of conventional enamelled wires. Kikuchi et al. (Kikuchi, 2002) emphasised that the inorganic/organic composite film can decrease erosion rate by increasing creeping distance and decreasing collision energy via reflection or scattering, as shown in Scheme 2.

Submicron spherical silica particles were added into the PAI polymer matrix during the synthesis of the silica/PAI composite films to evaluate the effects of silica diameter on their

properties. The characterisation results of the spherical silica/PAI composites are discussed as follows.

Fig. 8 shows the SEM micrographs of (a) the spherical silica submicron particles and (b) the fracture surface of the pure PAI and several spherical silica/PAI composite films. In Fig. 8 (a), the mean diameter of the spherical silica nanoparticles is about 300 nm, and most are well-dispersed after the surface modification process. The fracture surfaces of the pure PAI film are uniform, and the continuous polymer phase is shown in Fig. 8 (b). Figs. 8 (c)–(f) show the fracture surfaces of the different silica/PAI composites. The amount of silica added to the PAI was increased from 2 to 8 wt%. When the submicron spherical silica was added into the PAI matrix, some prominent features were observed on the fracture surfaces of the composite films, as shown in Fig. 8 (c). The spherical silica particles were embedded in the PAI matrix, and the continuous PAI organic phase appeared when the amount of silica added to the PAI was 2 and 4 wt%, as shown in Figs. 8 (c) and (d). When the amount of submicron silica increased, more spherical silica particles were observed on the fracture surfaces of the composite films. The continuous organic PAI phase separated, as shown in Fig. 8 (e). Some alveolate pores were observed in Fig. 8(f), when 8 wt% spherical silica was added into the PAI matrix. These pores are caused by the removal of the submicron silica particles from the PAI matrix when the composite films were broken.

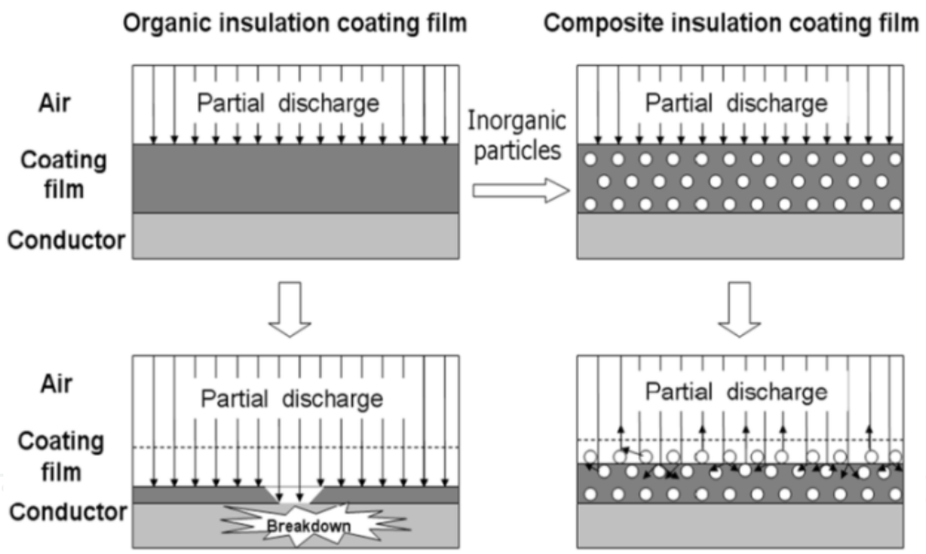

Scheme 2. Mechanism of erosion suppression.

More submicron spherical silica particles were subsequently added into the PAI matrix. The SEM micrographs of the composite film fracture surfaces are shown in Fig. 9. The micrographs show that the diameters of the submicron silica particles are uniform. In addition, the spherical silica particles are orderly arranged in the PAI matrix. An increase in the silica particles added into the films may result in a more compact framework. Partial discharge is a prime factor causing enamel wire breakdown, so the composite films caused a decrease in the erosion rate via reflection and scattering when the spherical silica particles were added into the PAI matrix. That is, the charged particles were reflected and scattered around the submicron silica, which slowed down the corrosion process. Therefore, the

particle discharge resistance is improved with the increase in silica content. When the amount of silica added to the PAI was increased to 25 wt%, as shown in Fig. 9 (d), the fracture surfaces of the composite films remained well-integrated without the obvious phase separation. The results indicate that such a simple method effectively increases the amount of inorganic silica particles in the PAI matrix after the surface modification process.

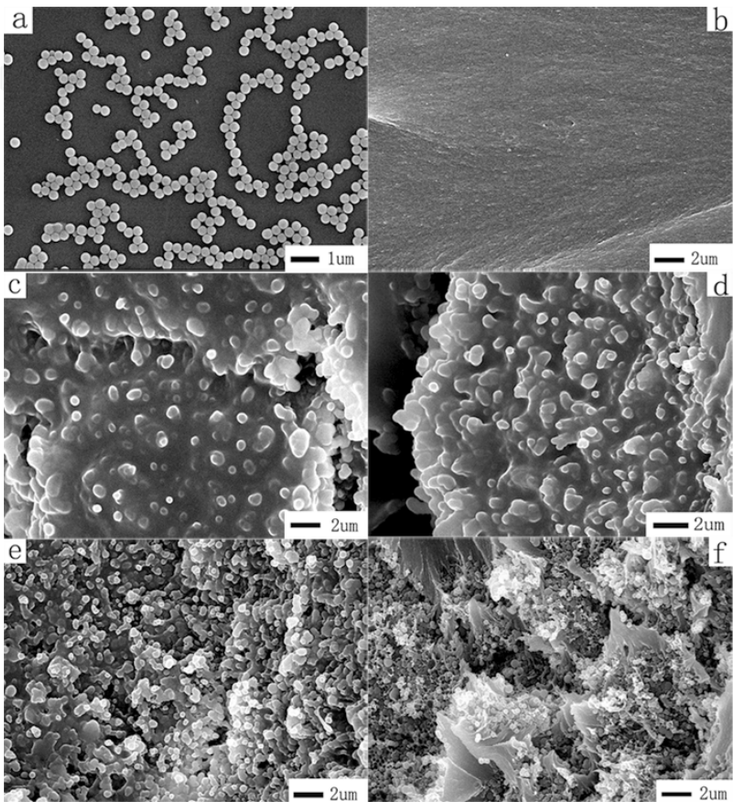

Fig. 8. SEM micrographs of (a) spherical silica submicron particles and fracture surfaces of (b) pure PAI film, (c) composite 1 with 2 wt% submicron silica, (d) composite 2 with 4 wt% submicron silica, (e) composite 3 with 6 wt% submicron silica, and (f) composite 4 with 8 wt% submicron silica.

The FT-IR spectra of CTAB-modified silica, pure PAI, and some submicron silica/PAI composite films are shown in Fig. 10. As shown in Fig. 3 (a), typical bands of silica were observed at 1086, 950, and 809 cm^{-1}, indicating the stretching vibrations of Si-O. The stretching vibration peaks of C-H were found at 2861 and 2915cm^{-1}, which came from the -CH_2 and -CH_3 in CTAB. The FT-IR spectra of PAI show the presence of the imide carbonyl band at 1776 and 1715 cm^{-1}, and the peaks at 3320 and 1715 cm^{-1} come from the N-H stretching and C=O region, respectively. Other characteristic bands include the absorption at 1600 cm^{-1} caused by the benzene ring stretch and a contribution from the O-H bond in monomeric H_2O, which also has a band at 1663 cm^{-1}. The bands at 950–650 and 3320 cm^{-1} increased with the increase in silica content. Furthermore, the adsorption peak at 1086 cm^{-1} was intensified in the spectra of the composites. All the characteristic peaks in the composites were insensitive to the presence of the silica component, indicating good interaction between the spherical silica and the PAI polymer matrix.

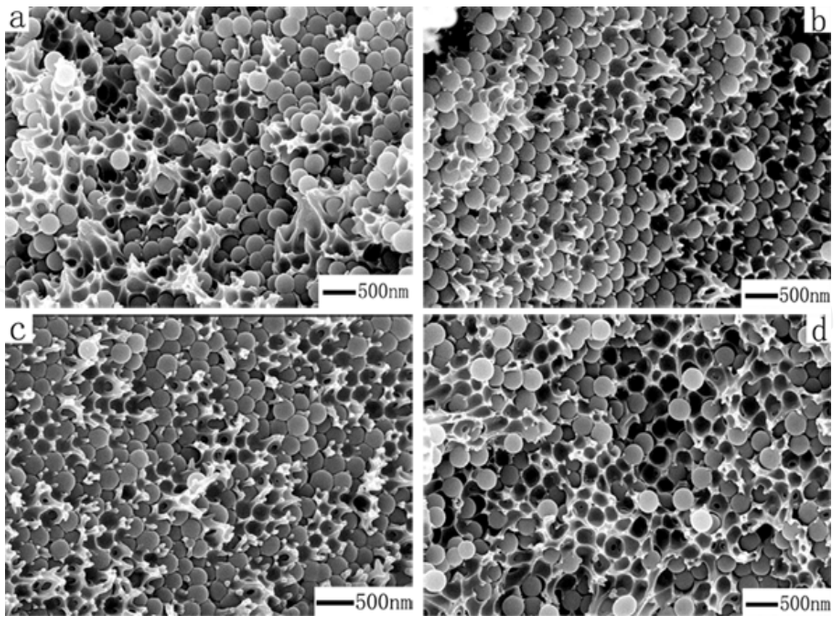

Fig. 9. SEM micrographs of (a) composite 5 with 10 wt% submicron silica, (b) composite 6 with 15 wt% submicron silica, (c) composite 7 with 20 wt% submicron silica, and (d) composite 8 with 25 wt% submicron silica.

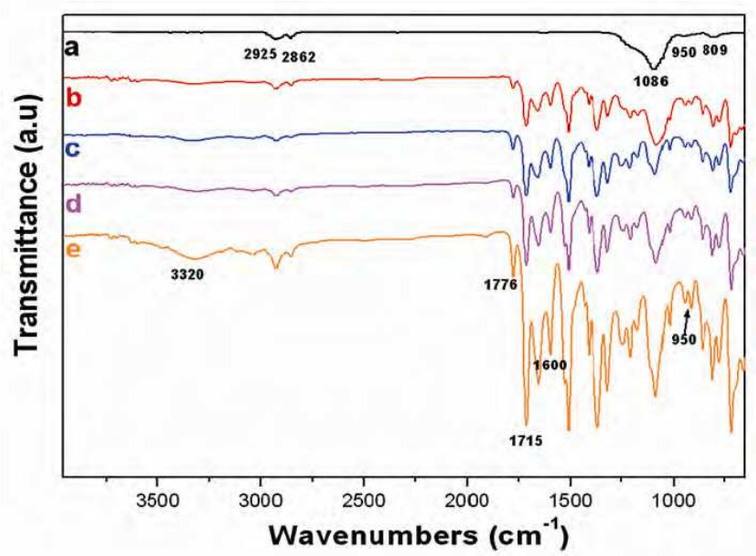

Fig. 10. FT-IR spectra of (a) CTAB-modified submicron silica particles, (b) pure PAI, (c) composite 1 with 2 wt% silica, (d) composite 2 with 4 wt% silica, and (e) composite 4 with 8 wt% silica.

The TGA plots of the PAI and the composites with the different amounts of submicron silica particles are shown in Fig. 11. Obvious weight loss is found in these plots. A weight loss is observed below 180 °C in all the TGA plots, corresponding to water and solvent losses. When the temperature was increased to 450 °C, the PAI matrix began to decompose with increasing decomposition temperature. The decomposition temperature increased from

640 to 678 °C after the silica particles were added to the PAI polymer matrix. The thermal stability of the PAI was increased by the incorporation of the submicron silica particles, as clearly shown in Fig. 11. The amount of silica particles in the composites were accurately calculated from the TGA plots. The silica content in the composites calculated based on the plots in Figs.11 (b)–(e) are 1.68, 3.80, 5.80, and 7.24 wt%. The calculated data are close to the theoretical values listed in Table 1.

Inorganic silica particles improve the thermal stabilities of the PAI polymer matrix and reduce the cost of enameled wire. To obtain the least expensive and most stable composite films, the amount of silica particles was increased from 10 to 25 wt%. In Fig. 12, the TGA curves are similar to the composite films shown in Fig. 11. The amount of silica particles was calculated based on the plots. The realistic data were 9.3, 13.7, 16.5, and 20.4 wt%.

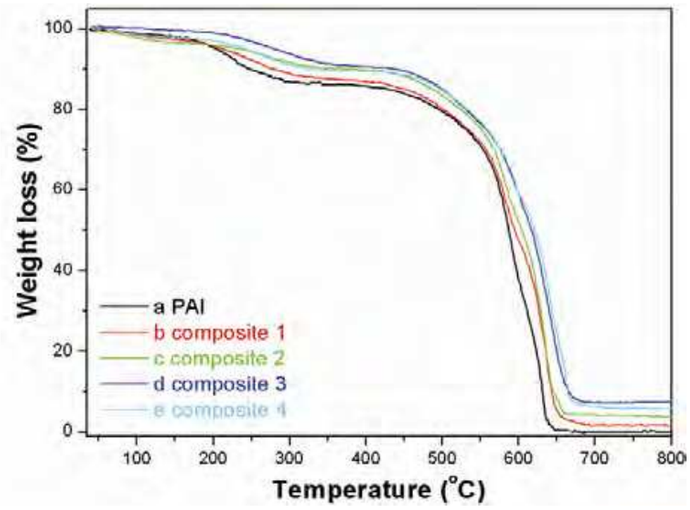

Fig. 11. TGA plots of (a) pure PAI, (b) composite 1 with 2 wt% silica, (c) composite 2 with 4 wt% silica, (d) composite 3 with 6 wt% silica, and (e) composite 4 with 8 wt% silica.

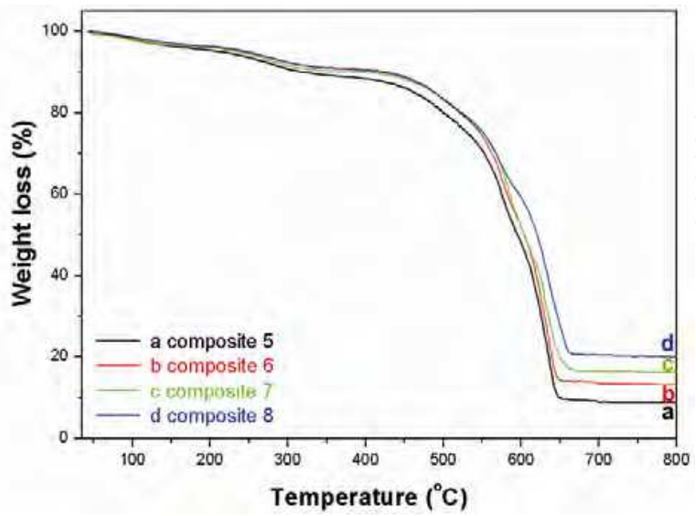

Fig. 12. TGA plots of (a) composite 5 with 10 wt% silica, (b) composite 6 with 15 wt% silica, (c) composite 7 with 20 wt% silica, and (d) composite 8 with 25 wt% silica.

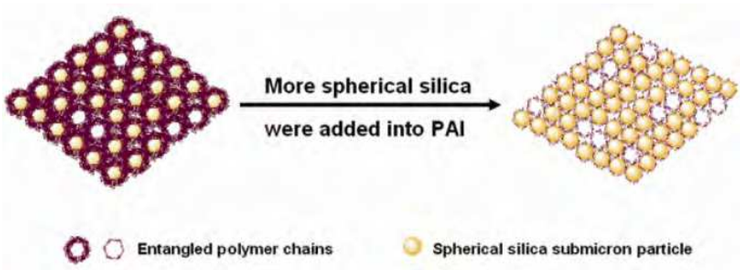

Scheme 3. Interactions between the silica submicron particles and the PAI polymer matrix.

Second, the thermal stability of the composite film was further improved by increasing the silica particles. However, the decomposition temperature was increased from 650 to 668 °C, the results of which did not exceed that of the composites shown in Fig. 11. These results indicate that the interaction between the silica and the PAI matrix changed when more silica submicron particles were added into the composite films. Initially, the thermal stability of PAI improved after the silica submicron particles were added into the PAI matrix. Given the thermal motion of molecules, the cohesion between the adjacent polymer chains and the partial resistance and friction from the incorporation of silica in the PAI matrix had to be overcome. When more silica submicron particles were added into the PAI polymer, the interaction between the silica and the PAI matrix weakened because of the more compact and orderly arrangement of silica in the PAI matrix, as shown in Scheme 3. In addition, the silica submicron particles were easier to break away from the fracture surfaces, as confirmed by the SEM micrographs shown in Fig. 9. As a result, the decomposition temperature of the composite film did not increase with increase in the amount of silica particles, when the amount of silica added to PAI was more than 10 wt%. However, the thermal stability and decomposition temperature of the composite film were obviously more prominent than those of the pure PAI polymer matrix. Considering the similar thermal stability and lower price of the enameled wire, the amount of silica submicron particles can be modulated from 4 to 25 wt%.

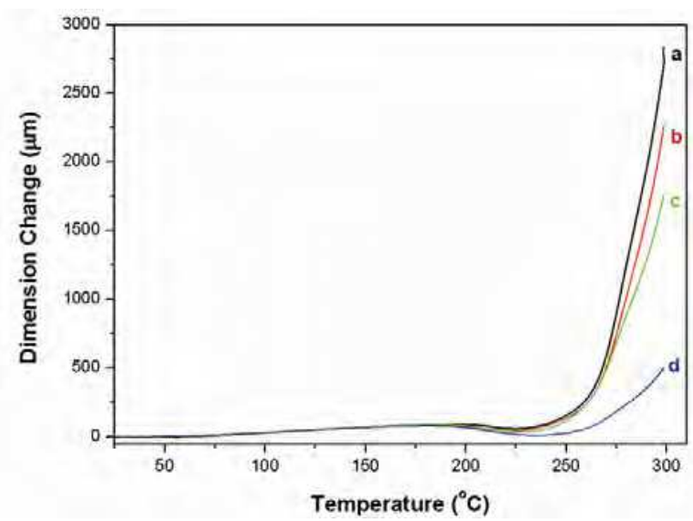

Fig. 13. CTE curves of the (a) pure PAI film, (b) composite 2 with 4 wt% silica, (c) composite 3 with 6 wt% silica, and (d) composite 6 with 15 wt% silica.

Controlling the CTE value of the dielectrical PAI is important because copper is the typical choice for defining the circuit lines. The selection of composites with the CTE close to that of copper is very critical, and can prevent damage to the copper interconnection; thus improving the reliability of the integrated circuits.

The CTE curves of the pure PAI film and some composite films are shown in Fig. 13. The CTE value of the pure PAI film is 3.87×10^{-5}m/m/°C, whereas that of the composite films in Figs. 13 (b)–(d) are 3.76×10^{-5}, 3.57×10^{-5}, and 3.25×10^{-5}m/m/°C, respectively. The CTE values continuously decreased with the increasing amount of the silica particles. The CTE value decreased by 16% when the amount of silica added to the PAI was 15 wt%. Such a variation in CTE is explained by the rigidity and stiffness of the silica submicron particles, which limit the movement of the polymer chain, resulting in the decrease of the thermal expansion of the PAI matrix. When the temperature increased to 220 °C, it approached the glass transition temperature of PAI. The dimension change significantly decreased with increased silica content. Therefore, the silica submicron particles effectively decrease the CTE value of the PAI polymer matrix, which in turn increases the thermal stress build-up, resulting in device failure through peeling and cracking at the interface between the PAI polymer film and the copper.

The thermal stability and the CTE value of the spherical silica/PAI composite films significantly improved when the submicron silica particles were added into the PAI polymer matrix. The submicron silica particles were obtained through the sol-gel method. Most previous studies used a sol-gel process because of the diameter of the silica particles. In the present study, the diameter effect was easily controlled using the Stőber procedure. Compared with the silica nanoparticles, the submicron silica particles have better dispersal state and do not easily agglomerate. Thus, more submicron silica particles are well-dispersed in the PAI polymer matrix after the surface modification process. Considering the higher thermal stability and lower CTE value, especially the lower cost, submicron silica/PAI composite films can be widely used in the enamel wire industry.

3. Conclusion

In the current work, silica particles with two different diameters were successfully added into the PAI polymer matrix in the synthesis of silica/PAI composite films via simple ultrasonic blending. First, the effect of CTAB on the synthesis of the silica/PAI composite film was investigated. The optimal dosage of CTAB is 3 wt%. The fracture surface micrographs of the composites show that the silica nanoparticles are well-dispersed in the PAI matrix after the surface modification process. In the TGA plots of the silica/PAI nanocomposites, the thermal stability and the decomposition temperature obviously increased with increasing CTAB dosage. Therefore, CTAB improves not only the dispersal state of silica in the PAI matrix, but also the thermal stability of the composite film because of better interaction between the nanosilica and the PAI matrix.

When the amount of silica nanoparticles added to the PAI was increased from 2 to 10 wt%, the thermal stability of the silica/PAI nanocomposites improved. The decomposition temperature increased with the increase in the amount of silica nanoparticles. In particular, the CTE value decreased when the silica particles were added

into the PAI matrix. The CTE value further decreased with the increase in the amount of silica nanoparticles. When the submicron silica particles were added into the PAI polymer matrix, a similar conclusion was reached. However, more submicron silica particles are well-dispersed in the PAI polymer matrix after the surface modification process because the submicron silica particles have better dispersal state. Considering the higher thermal stability, lower CTE value, and the lower cost, silica/PAI composite films can be widely used in the enamel wire industry.

4. Acknowledgement

This research was supported by Basic Science Research Program through the National Research Foundation of Korea (NRF) Funded by the Ministry of Education, Science and Technology. (No. 2011-0016699). Also, it was supported by Sanhak Fellowship program funded of Korea Sanhak foundation.

5. References

Ahn, B. Y.; Seok, S. I.; Hong, S.; Oh, J.; Jung, H.; Chung, W. J. (2006). Optical properties of organic/inorganic nanocomposite sol-gel films containing $LaPO_4$:Er,Yb nanocrystals. *Optical Materials*, 28, 4, pp. 374-379

Alexandre, M.; Dubois, P. (2000). Polymer-layered silicate nanocomposites: preparation, properties and uses of a new class of materials. *Materials Science and Engineering*, 28, 1-2, pp. 1-63

Babooram, K.; Francis, B.; Bissessur, R.; Narain R. (2008). Synthesis and characterization of novel (amide–imide)-silica composites by the sol–gel process. *Composites Science and Technology*, 68, 3-4, pp. 617–624

Bhagat, S. D.; Kim, Y.; Suh, K.; Ahn, Y.; Yeo, J.; Han, J. (2008). Superhydrophobic silica aerogel powders with simultaneous surface modification, solvent exchange and sodium ion removal from hydrogels. *Microporous and Mesoporous Materials*, 112, 1-3, pp. 504-509

Butterworth, M. D.; Corradi, R.; Johal, J.; Lascelles, S. F.; Maeda, S.; Armes, S. P. (1995). Zeta Potential Measurements on Conducting Polymer-Inorganic Oxide Nanocomposite Particles. *Journal of Colloid and Interface Science*, 174, 2, pp. 510-517

Castellano, M.; Conzatti, L.; Costa, G.; Falqui, L.; Turturro, A.; Valenti, B.; Negroni, F. (2005). Surface modification of silica: 1. Thermodynamic aspects and effect on elastomer reinforcement. *Polymer*, 46, 3, pp. 695-703

Chen, L. W.; Ho, K. S. (1997). Synthesis of Polyamide-imide by Blocked-Methylene Diisocyanates. *Journal of Polymer Science Part A: Polymer Chemistry*, 35, 9, pp. 1711-1717

David, I. A.; Scherer, G. W. (1995). An Organic/Inorganic Single-Phase Composite. *Chemistry of Materials*, 7, pp. 1957-1967

Fuchigami, K.; Taguchi, Y.; Tanaka, M. (2008) Synthesis of spherical silica particles by sol-gel method and application. *Polymer for Advanced Technologies*, 19, pp. 977–983

Hossein, S. S.; Lia, Y.; Chunga, T.; Liu, Y. (2007). Enhanced gas separation performance of nanocomposite membranes using MgO nanoparticles. *Journal of Membrane Science*, 302, 1-2, pp. 207–217

Hwang, J.; Lee, B. I.; Klep, V.; Luzinov, I. (2008). Transparent hydrophobic organic–inorganic nanocomposite films. *Materials Research Bulletin*, 43, 10, pp. 2652-2657

Jadav, G. L.; Singh, P. S. (2009). Synthesis of novel silica-polyamide nanocomposite membrane with enhanced properties. *Journal of Membrane Science*, 328, 1-2, pp. 257-267

Jiao, W. M.; Vidal, A.; Papirer, E.; Donnet, J.B. (1989). Modification of Silica Surfaces by Grafting of Alkyl Chains Part III. Particle/Particle Interactions: Rheology of Silica Suspensions in Low Molecular Weight Analogs of Elastomers. *Colloids and Surfaces*, 40, pp. 279-291

Kawakami, H.; Mikawa, M.; Nagaoka, S. (1996). Gas permeability and selectivity through asymmetric polyimide membranes. *Journal of Appled Polymer Science*, 62, 7, pp. 965–971

Kawakami, H.; Mikawa, M.; Nagaoka, S. (1998). Gas transport properties of asymmetric polyimide membrane with an ultrathin surface skin layer. *Macromolecules*, 31, 19, pp. 6636–6638

Kawakami, H.; Nakajima, K.; Shimizu, H.; Nagaoka S. (2003). Gas permeation stability of asymmetric polyimide membrane with thin skin layer: effect of polyimide structure. *Journal of Membrane Science*, 212, 1-2, pp. 195–203

Kikuchi, H.; Yukimon, Y.; Itonaga, S. (2002). Inverter-surge-resistant enameled wire based on nano-composite insulating material. *Hitachi Cable Review*, 21, pp. 55-62

Kim, J. Y.; Mulmi, S.; Lee, C. H.; Park, H. B.; Chung, Y. S.; Lee, Y. M. (2006). Preparation of organic–inorganic nanocomposite membrane using a reactive polymeric dispersant and compatibilizer: Proton and methanol transport with respect to nano-phase separated structure. *Journal of Membrane Science*, 283, 1-2, pp. 172-181

Kim, T. K.; Kang, M.; Choi, Y. S .; Kim, H. K.; Lee, W.; Chang, H.; Seung, D. (2007). Preparation of Nafion-sulfonated clay nanocomposite membrane for direct menthol fuel cells via a film coating process. *Journal of Power Sources*, 165, 1, pp. 1-8

Kusakabe, K.; Ichiki, K.; Hayashi, J.; Maeda, H.; Morooka, S. (1996). Preparation and characterization of silica-polyimide composite membranes coated on porous tubes for CO_2 separation. *Journal of Membrane Science*, 115, 1, pp. 65-75

Lee, Y. L.; Du, Z. C.; Lin, W. X.; Yang, Y. M. (2006). Monolayer behavior of silica particles at air/water interface:A comparison between chemical and physical modifications of surface. *Journal of Colloid Interface Science*, 296, 1, pp. 233-241

Ma, J.; Yang, Z.; Wang, X.; Qu, X.; Liu, J.; Lu, Y.; Hu, Z.; Yang, Z. (2007). Flexible bi-continuous mesostructured inorganic/polymer composite membranes. *Polymer*, 48, 15, pp. 4305-4310

Mosher, B. P.; Wu, C.; Sun, T.; Zeng, T. (2006). Particle-reinforced water-based organic-inorgaic aocomposite coatings for tailored applications. *Journal of Non-Crystalline Solids*, 352, 30-31, pp. 3295-3301

Oh, C.; Lee, Y. G.; Jon, C. U.; Oh, S. G. (2009). Synthesis and characterization of hollow silica microspheres functionalized with magnetic particles using W/O emulsion method. *Colloids and Surfaces A: Physicochemical and Engineering Aspects*, 337, 1-3, pp. 208-212

Ohki, Y. (2005). Study on dielectric properties of LDPE-based nanocomposites by J-power systems. *IEEE Electrical Insulation Magazine*, 21, 3, pp. 55-56

Ouabbas, Y.; Chamayou, A.; Galet, L.; Baron, M.; Thomas, G.; Grosseau, G.; Guilhot, B. (2009). Surface modification of silica particles by dry coating: Characterization and powder aging. *Powder Technology*, 190, 1-2, pp. 200-209

Ranade, A.; Souza, N.; Gnade, B. (2002). Exfoliated and intercalated polyamide-imide nanocomposites with montmorllonite. *Polymer*, 43, 13, pp. 3759-3766

Rangsunvigit, P.; Imsawatgul, P.; Na-ranong, N.; O'Haver, J. H.; Chavadej, S. (2008) Mixed surfactants for silica surface modification by admicellar polymerization using a continuous stirred tank reactor. *Chemical Engineering Journal*, 136, 2-3, pp. 288-294

Rankin, S. E.; Macosko, C. W.; McCormick, A. V. (1998). Sol-Gel Polycondensation Kinetic Modeling: Methylethoxysilanes. *AIChE Journal*, 44, 5, pp. 1141-1156

Rupnowski, P.; Gentz, M.; Kumosa, M. (2006). Mechanical response of a unidirectional graphite fiber /polyimide composite as a function of temperature. *Composites Science and Technology*, 66, 7-8, pp. 1045–1055

Stathatos, E.; Lianos, P.; Tsakiroglou, C. (2004). Highly efficient nanocrystalline titania films made from organic/inorganic nanocomposite gels. *Microporous and Mesoporous Materials*, 75, 3, pp. 255-260

Sun, S.; Li, C.; Zhang L.; Du, H.L.; Burnell-Gray J.S. (2006). Effects of surface modification of fumed silica on interfacial structures and mechanical properties of poly(vinyl chloride) composites. *European Polymer Journal*, 42, 7, pp. 1643-1652

Wu, J.; Yang, S.; Gao, S.; Hu, A.; Liu, J.; Fan, L. (2005). Preparation, morphology and properties of nano-sized Al_2O_3/polyimide hybrid films. *European Polymer Journal*, 41, 1, pp. 73-81

Wu, T.; Ke, Y. (2006). Preparation of silica–PS composite particles and their application in PET. *European Polymer Journal*, 42, 2, pp. 274-285

Xu, J.; Wong, C.P. (2007). Characterization and properties of an organic–inorganic dielectric nanocomposite for embedded decoupling capacitor applications. *Composites Part A: Applied Science and Manufacturing*, 38, 1, pp. 13-19

Xue, L.; Li, J.; Fu, J.; Han, Y. (2009). Super-hydrophobicity of silica nanoparticles modified with vinyl groups. *Colloids and Surfaces A: Physicochemical and Engineering Aspects*, 338, 1, pp. 15-19

Yang, Y.; Wang, P. (2006). Preparation and characterizations of a new PS/TiO_2 hybrid membrane by sol–gel process. *Polymer*, 47, 8, pp. 2683–2688

Yanagishita, H.; Kitamoto, D.; Haraya, K.; Nakane, T.; Okada, T.; Matsuda, H.; Idemoto, Y.; Koura N. (2001). Separation performance of polyimide composite membrane prepared by dip coating process. *Journal of Membrane Science*, 188, 2, pp.165–172

Zhang, C.; Zhang, M.; Cao, H.; Zhang, Z.; Wang, Z.; Gao, L.; Ding, M. (2007). Synthesis and properties of a novel isomeric polyimide/SiO_2 hybrid material. *Composites Science and Technology*, 67, 3-4, pp. 380-389

Zheng, P.; Kong L. X.; Li, S.; Yin, C.; Huang M. F. (2007). Self-assembled natural rubber/silica nanocomposites: Its preparation and characterization. *Composites Science and Technology*, 67, 15-16, pp. 3130-3139

Zhong, S.; Li, C .; Xiao, X. (2002). Preparation and characterization of polyimide–silica hybrid membranes on kieselguhr–mullite supports. *Journal of Membrane Science*, 199, 1-3, pp. 53–58

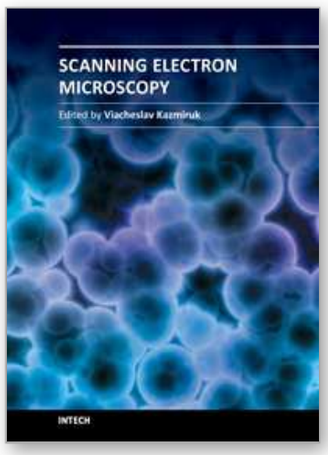

Scanning Electron Microscopy

Edited by Dr. Viacheslav Kazmiruk

ISBN 978-953-51-0092-8

Hard cover, 830 pages

Publisher InTech

Published online 09, March, 2012

Published in print edition March, 2012

Today, an individual would be hard-pressed to find any science field that does not employ methods and instruments based on the use of fine focused electron and ion beams. Well instrumented and supplemented with advanced methods and techniques, SEMs provide possibilities not only of surface imaging but quantitative measurement of object topologies, local electrophysical characteristics of semiconductor structures and performing elemental analysis. Moreover, a fine focused e-beam is widely used for the creation of micro and nanostructures. The book's approach covers both theoretical and practical issues related to scanning electron microscopy. The book has 41 chapters, divided into six sections: Instrumentation, Methodology, Biology, Medicine, Material Science, Nanostructured Materials for Electronic Industry, Thin Films, Membranes, Ceramic, Geoscience, and Mineralogy. Each chapter, written by different authors, is a complete work which presupposes that readers have some background knowledge on the subject.

InTech Europe
University Campus STeP Ri
Slavka Krautzeka 83/A
51000 Rijeka, Croatia
Phone: +385 (51) 770 447
Fax: +385 (51) 686 166
www.intechopen.com

InTech China
Unit 405, Office Block, Hotel Equatorial Shanghai
No.65, Yan An Road (West), Shanghai, 200040, China
中国上海市延安西路65号上海国际贵都大饭店办公楼405单元
Phone: +86-21-62489820
Fax: +86-21-62489821

IntechOpen